Optics & Laser Technology 170 (2024) 110211

Contents lists available at ScienceDirect

Optics and Laser Technology

journal homepage: www.elsevier.com/locate/optlastec

Full length article

Linear polarization and narrow-linewidth external-cavity semiconductor laser based on birefringent Bragg grating optical feedback

Jiaqi Chen [a,b], Chao Chen [a,b,c,*], Qi Guo [d], Jingjing Sun [a], Jianwei Zhang [a], Yinli Zhou [a], Zhaohui Liu [a], Yongsen Yu [d], Li Qin [a,c], Yongqiang Ning [a,c], Lijun Wang [a]

[a] State Key Laboratory of Luminescence and Application, Changchun Institute of Optics, Fine Mechanics and Physics, Chinese Academy of Sciences, Changchun 130033, China
[b] University of Chinese Academy of Sciences, Beijing 100049, China
[c] Xiongan Innovation Institute, Chinese Academy of Sciences, Xiongan 071800, China
[d] State Key Laboratory of Integrated Optoelectronics, College of Electronic Science and Engineering, Jilin University, Changchun 130012, China

ARTICLE INFO

Keywords:
Semiconductor laser
Narrow linewidth
Linear polarization
Birefringent Bragg grating

ABSTRACT

We demonstrate an external-cavity semiconductor laser (ECSL) with linear polarization and a narrow linewidth. A birefringent Bragg grating prepared by a femtosecond laser point-by-point technique in a polarization-maintaining fiber (PMF) is used to provide external-cavity feedback, and its polarization-dependent characteristics enable selection of the main polarization mode and linewidth narrowing of the ridge waveguide emission gain chip (GC). This compact and robust ECSL achieves an output power of $>$ 60 mW and a polarization extinction ratio (PER) of $>$ 30 dB. We simulate and calculate the linewidth and injection current, while a Lorentz linewidth of 2.58 kHz is obtained based on delayed self-heterodyne beat frequency measurement. This flexible and cost-effective solution allows realization of a compact ECSL with linear polarization and a narrow linewidth.

1. Introduction

Quantum precision measurement realizes the characterization of time [1], magnetism [2], inertia [3], gravitational waves [4] and other physical quantities through atomic polarization, spin, squeezed states and coherent states, which are based on the interaction of light, magnetism and atoms. These applications require narrow-linewidth lasers to meet the fine-level transitions for the detection of atoms [5], while high polarization of the lasers helps improve the performance of the Pound–Drever–Hall frequency stabilization system and the interference system, achieving high-precision and high-resolution precision measurements [6]. Therefore, compact lasers with a narrow linewidth and linear polarization have received widespread attention from researchers.

The wavelengths of the required lasers are mainly concentrated in the near-infrared band [1–6] for quantum precision measurement applications represented by atomic clocks, atomic magnetometers and atomic gyroscopes; such as 795 nm and 780 nm correspond to Rb D1 and D2 lines, while 894 nm and 852 nm correspond to Cs D1 and D2 lines. Narrow-linewidth lasers such as monolithic integration, external-cavity, and frequency doubling lasers, have been proposed [7–16] based on the classical Schawlow-Townes linewidth theory [7]. Distributed-feedback (DFB) and distributed Bragg reflector (DBR) lasers can achieve a linewidth of 100 kHz by optimizing the grating coupling coefficient and cavity length [8,9]. However, the chip length limits further narrowing of the linewidth, while secondary epitaxy and high lithography accuracy increase the complexity and cost. A kHz linewidth can be obtained for external-cavity semiconductor lasers (ECSLs) by extending the length of the resonant cavity, which is based on volume holographic Bragg gratings, blazed gratings and filters [10–15]. However, the high complexity of adjustment and limited mechanical stability can easily cause wavelength detuning due to vibration. The frequency-doubling laser scheme based on the second harmonic effect [16] has a more complex structure and is constrained by the frequency conversion efficiency. The above schemes can achieve a polarization extinction ratio (PER) of approximately 20 dB, while a higher PER requires the introduction of an external passive polarization controller [17].

An ECSL based on selective polarization mode feedback provides a solution for narrow-linewidth and linear polarization lasers, in which optical feedback and mode locking are achieved through birefringent

* Corresponding author.
E-mail address: chenc@ciomp.ac.cn (C. Chen).

https://doi.org/10.1016/j.optlastec.2023.110211
Received 7 August 2023; Received in revised form 7 October 2023; Accepted 11 October 2023
Available online 14 October 2023

Bragg gratings [18]. External-cavity lasers with fiber Bragg gratings (FBGs) have advantages in integration and performance. The equivalent resonant cavity structure can be optimized to synchronously achieve linewidth narrowing and active polarization control by designing gain chip (GC) and FBGs, respectively [19]. The GC does not involve the fabrication of a nanoscale grating, which can avoid the introduction of additional transmission losses into the active waveguide. A mature FBG design method allows customization of the Bragg resonance wavelength, reflection bandwidth, and reflectivity [20]. These are beneficial for cost control and large-scale production of lasers. However, the FBG-ECSL puts forward new requirements for the birefringence characteristics of Bragg gratings, considering both a narrow linewidth and linear polarization. A femtosecond laser induces shape asymmetry and refractive index asymmetry of the grating waveguide structure in a transparent medium, which can introduce a strong birefringence effect [21]. These phenomena provide the potential for the preparation of high-birefringence Bragg gratings and their applications in polarization lasers [22].

In this work, we demonstrate an ECSL with a narrow linewidth and linear polarization based on an external optical feedback structure. A birefringent Bragg grating induced by a femtosecond laser provides feedback and selection of the main polarization mode of the GC. Single-frequency output and linewidth compression are achieved by expanding the length of the laser resonant cavity. The Lorentz linewidth is as small as 2.58 kHz under the condition of ensuring an output power of over 60 mW, while the PER is 30.25 dB. The proposed laser structure is more compact and more integrated than the traditional Littrow and Litman structures of ECSLs. The laser can be used as a potential alternative to the atomic pump light source in quantum precision measurement applications, and it is promising for cold atom quantum experiments in space environments.

2. Laser structure

A schematic diagram of the ECSL is shown in Fig. 1 (a). It consist of a ridge waveguide emission GC and a birefringent Bragg grating, which

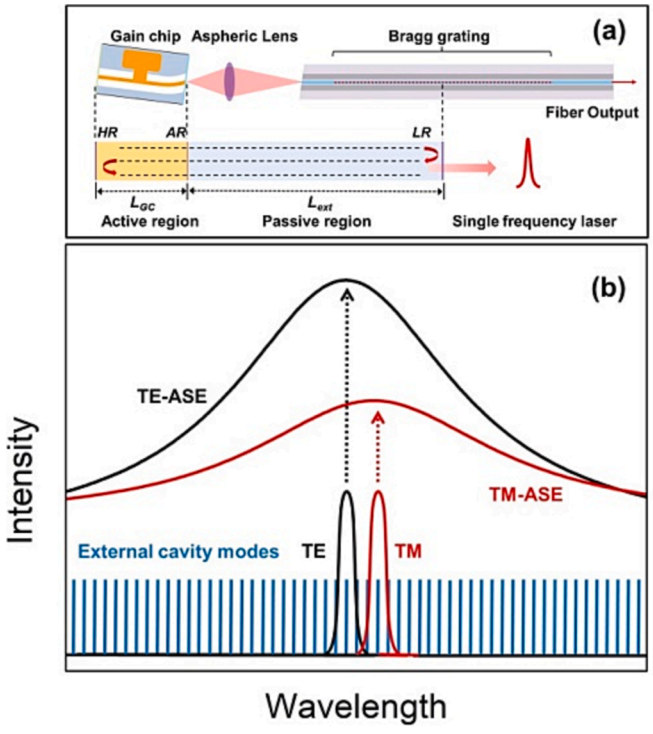

Fig. 1. (a) Schematic diagram of the ECSL. (b) Principle of the frequency selection for the equivalent resonant cavity.

are coupled and integrated through an aspheric lens, and they are all installed on a thermoelectric cooler (TEC) for thermal management. There are also some other components inside the laser, such as thermistors and photonic diodes. A resonator is formed between the facet of the GC and the equivalent center of the Bragg grating. The GC has a compressive strain quantum well to provide stronger transverse electric (TE) mode gain and suppress transverse magnetic (TM) mode amplified spontaneous emission. The linear polarization output comes from the orthogonal polarization eigenmode and effective selection of the external-cavity mode of the birefringent FBG [23]. Polarization-dependent characteristics of the birefringent Bragg grating are achieved via femtosecond laser-induced refractive index modulation and morphology modulation [21]. The polarization- dependent characteristics of the birefringent Bragg grating support selection of the TE mode of the GC and linewidth narrowing, as shown in Fig. 1 (b). The feedback is returned to the GC to achieve a higher mode gain difference in the locked mode. In addition, the input facet of the fiber is cleaved at an angle of 8° to reduce the reflectivity. The metallized aspheric lens and Bragg grating are fixed by laser welding to enhance the stability of the device. All components are integrated into a standard 14-pin butterfly-shaped package.

An ECSL can be equivalent to the combination of an active gain region and a passive external cavity. The free spectral range (FSR) of the equivalent resonant cavity is 18.6 pm, and its effective reflectivity R_{eff} mainly depends on the FBG reflectivity and transit time τ_e, where $\tau_e = 2n_{ext}L_{ext}/c$. The linewidth characteristics of the laser often involve factors such as the photon lifetime and feedback delay, so the resonator cavity is regarded as an isolated laser with fixed mode spacing [24]:

$$\Delta v = \frac{R_{sp}(1+\alpha^2)}{P}\left(\frac{n_{GC}L_{GC}}{n_{GC}L_{GC}+n_{ext}L_{ext}}\right)^2 \quad (1)$$

where R_{sp} is the spontaneous emission rate, α is the linewidth enhancement coefficient, and $n_{ext}(L_{ext})$ is the effective refractive index (cavity length) of the external cavity. The relationship between the output power and the current can be expressed as [25]:

$$P = \frac{I - I_{th}}{q\Gamma a v_g (N - N_0)} \quad (2)$$

where q is the amount of charge, Γ is the constraint factor, a is the differential gain, v_g is the group velocity, and I_{th} is the threshold current.

A longer resonant cavity length prolongs the photon lifetime, which is beneficial for narrowing the linewidth. The linewidth of the laser decreases with increasing current when the other parameters are constant, and spontaneous emission tends to stabilize after laser lasing and gradually approaches the minimum value. This is confirmed in the subsequent discussion on the linewidth testing results.

The InGaAs quantum well GC adopts a bent ridge waveguide structure, with a chip length (L_{GC}) of 1.50 mm [26,27], and the narrow ridge waveguide can meet the single-mode cutoff condition and ensure a single-transverse-mode output, while the double groove can reduce the lateral diffusion of the driving current. The waveguide near the output face has an inclination angle of 7° to reduce the influence of chip cavity modes on resonant cavity frequency selection. The power–current–voltage (P-I-V) characteristics in continuous operation of the GC are shown in Fig. 2 (a), and an output power of 30 mW and a slope efficiency of 0.14 W/A are achieved for the antireflection (AR)/high-reflectivity (HR)-coated facet chip. The amplified spontaneous emission (ASE) spectra of different currents were tested, and the chip could achieve a wide gain range of approximately 850 nm, as shown in Fig. 2 (b).

The polarization characteristics of the GC were analyzed to clarify its impact on the polarization output of the laser. We tested the polarization characteristics of the GC by using a linear polarization controller (Thorlabs, FBR-LPNIR), a tunable fiber-to-fiber coupler (Thorlabs, FBP-C-FC), and a power meter (Thorlabs, PM400) [28,29]. The relationship

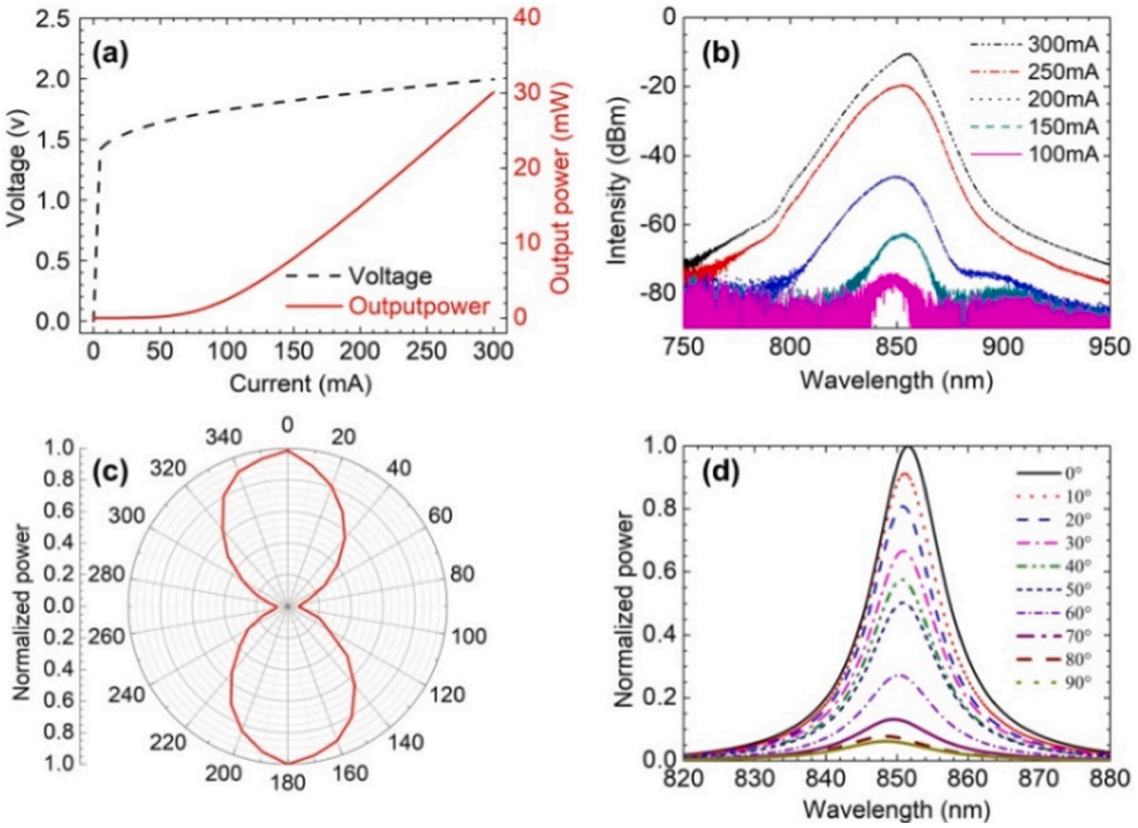

Fig. 2. (a) P-I-V characteristics and (b) ASE spectra of the GC; normalized (c) power versus angle and (d) shift of the ASE peak due to varying the polarization from the TE to TM modes.

between the normalized output power of the GC and the rotation angle can be obtained, as shown in Fig. 2 (c). The output light of the GC achieves a PER of 11.68 dB after passing through the polarization controller. Fig. 2 (d) shows the ASE spectra of the GC at different polarization rotation angles. These results indicate that the quantum well chip itself has certain polarization characteristics, and the shift in the ASE peak caused by the polarization change from the TM mode to the TE mode is due to the compressive strain effect of the quantum wells [30]. The compressive strain makes the heavy-hole band higher than the light-hole band in the valence band based on the relationship between the lattice mismatch and strain of semiconductor materials. Carrier recombination between the first conduction band and the first heavy-hole valence band dominates, which produces the TE mode, and its gain dominates. This is more conducive to the selection of the TE mode by the birefringent Bragg grating, which achieve a larger mode gain difference and improve the overall PER of the laser.

The birefringent Bragg grating was prepared in a polarization-maintaining fiber (PMF) (Corning PM780) using femtosecond laser point-by-point lithography technology [31,32], as shown in Fig. 3 (a). Femtosecond laser lithography along the fast axis direction can enhance the birefringence effect. In addition, lithography along the fast axis direction can also avoid the stress zone in the PMF, as the stress zone might change the focusing optical path and reduce the processing quality [33]. All components are coaxial, which allows the FBG to achieve fixed and polarization rotation alignment. The FBG has a length (L_{FBG}) of 6.00 mm and a period (Λ) of 880 nm. The blue curve in Fig. 3 (b) is the reflection spectrum, and the black curve is the transmission spectrum. Two peaks occur in the reflection spectrum at 852.56 nm and 852.85 nm, corresponding to a 3 dB bandwidth of 50 pm, respectively. The wavelength difference between the two modes is 0.29 nm, and the birefringence is $1.65\text{x}10^{-4}$ ($\Delta n_{eff}^{TM-TE} = \Delta\lambda_B^{TM-TE}/2\Lambda$), which is an order of magnitude larger than that of the ultraviolet-written grating [34]. A larger

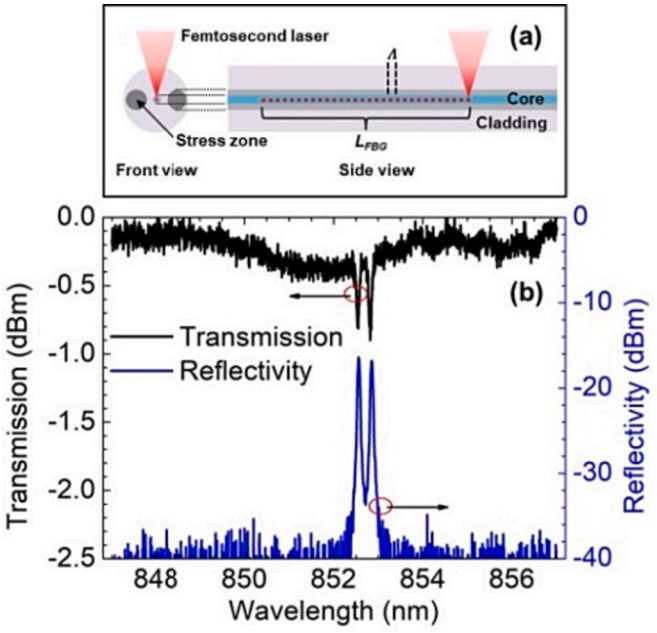

Fig. 3. (a) Schematic diagram of the device for fabricating FBGs. (b) Reflection and transmission spectra of the Bragg gratings.

wavelength difference (birefringence) is beneficial for increasing the gain difference of the polarization modes and obtaining a higher PER of the laser. The side mode suppression ratio (SMSR) is an important indicator for measuring the single-frequency performance of narrow-linewidth lasers. The SMSRs of the two modes are 18.46 dB and

18.04 dB, with reflectivities of 17.05 % and 18.68 %. A lower reflectivity ensures a high output power.

3. Results and discussion

The device was butterfly packaged, while precise current and temperature control of the laser was achieved using an ultralow noise current source (LDX-3620B, ILX Lightwave Corporation) and a TEC (LDT-5910C, ILX Lightwave Corporation). A low-pass filter (LNF-320, ILX Lightwave Corporation) was applied to further suppress ripple noise. The lasing spectra were measured with a spectral analyser (AQ6370B, Yokogawa), the resolution was set to 20 pm, and the TEC was set to 25 °C.

3.1. Spectra and power–current–voltage characteristics

Fig. 4 (a) shows the lasing spectra of the laser under different injection currents, and a color map of the spectra as a function of the injection currents is shown in Fig. 4 (b). The injection current is changed from 50 mA to 300 mA, with the spectra at 50 mA (black curve) and 54 mA (red curve) showing the lasing process around the threshold point. The laser clearly always maintains a single longitudinal mode and a single transverse mode according to the spectral characteristics in Fig. 4. In addition, the beat frequency spectrum obtained in the linewidth characterization based on the delayed self-heterodyne beat frequency measurement discussed in the following text also only displays the frequency components of a single frequency. The laser achieves an SMSR of 55.42 dB at 852.5247 nm when the injection current reaches 300 mA. A higher SMSR can reduce mode hopping and improve the single-longitudinal-mode tuning range, and it can also reduce the bandwidth of the laser spectrum. The AR coating of the GC can effectively suppress its cavity mode and increase the SMSR.

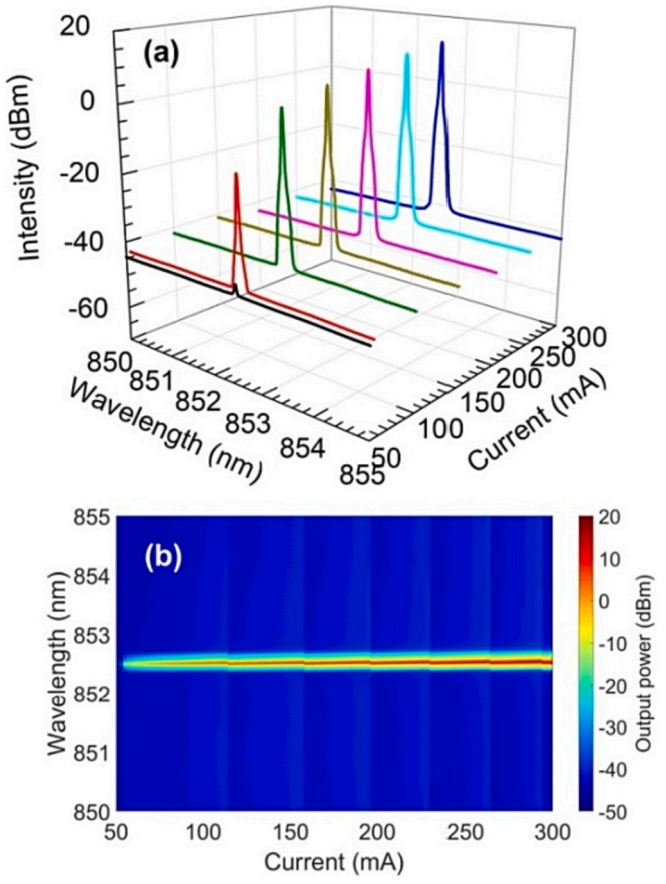

Fig. 4. Lasing spectra versus injection current: (a) spectra obtained using different currents and (b) jet map of the optical spectra as a function of the injection currents.

The P-I-V characteristics in Fig. 5 (a) show a threshold current of 54 mA and a maximum output power of 61.22 mW, with a corresponding slope efficiency of 0.24 W/A. Fig. 5 (b) shows the changes in the SMSR and wavelength corresponding to Fig. 4. The variation in the laser wavelength with the injection current is caused by temperature-induced refractive index changes, and the wavelength sensitivity coefficient continuously increases from 0.44 nm/A at 50 mA to 0.56 nm/A at 300 mA. The continuous wavelength tuning range of the laser is approximately 18 pm, which is basically consistent with the FSR of the equivalent resonant cavity. Meanwhile, the SMSR in Fig. 5 (b) also shows periodic changes with increasing injection current, with a decrease in the SMSR within a continuous tuning range, which means a lower adjacent mode gain differences and a higher output power. An inflection point in the curve corresponds to a mode jump, which is due to the mismatch between the equivalent cavity mode and the Bragg resonant mode.

3.2. Polarization characteristics

The polarization characteristics of the laser were tested using the same devices and method as those used for the GC [28,29]. The polar coordinates of the output power and the polarization rotation angle are shown in Fig. 6 (a). The maximum power (P_{max}) and the minimum power (P_{min}) at 300 mA are 46.24 mW and 43.65 μW, respectively, and the corresponding PER is 30.25 dB (PER $= 10log_{10}(P_{max}/P_{min})$). Fig. 6 (b) shows the spectra at different rotation angles, and the fluctuation of the curves may be due to the interference effect when the light passes through the polarization controller. The PERs under different currents

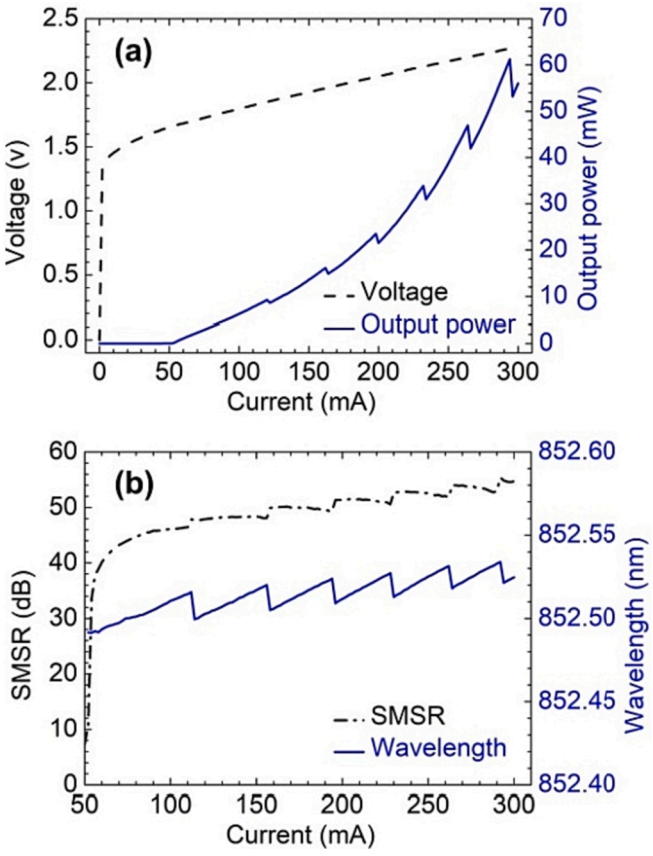

Fig. 5. (a) P-I-V curve of the laser. (b) SMSR and wavelength versus injection current.

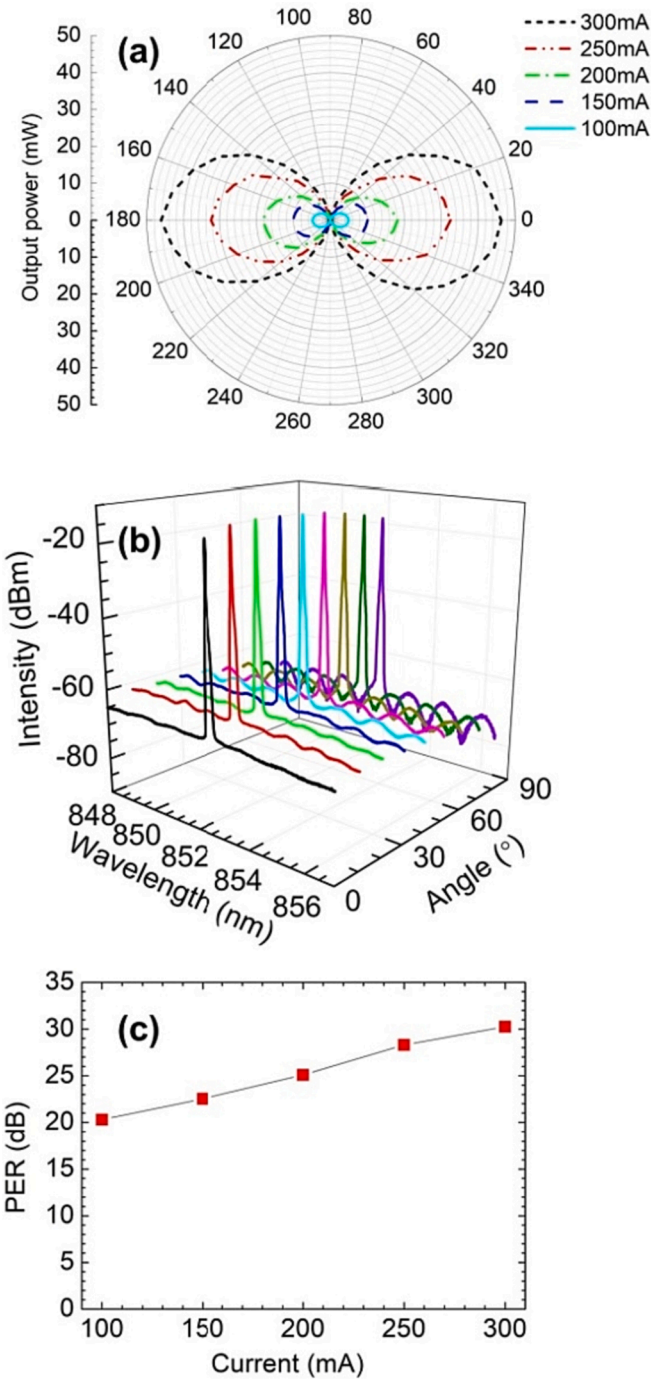

Fig. 6. (a) Output power versus rotation angle of the laser. (b) Spectra at different polarization angles. (c) PER value at different currents.

are shown in Fig. 6 (c). An increase in the injection current leads to a larger gain in the GC, resulting in a higher mode gain difference. The power conversion efficiency of the TE mode is higher than that of the TM mode, and the corresponding PER also increases with increasing injection current. The laser achieves a PER of > 30 dB, exhibiting great TE mode linear polarization, and the TM mode is fully suppressed. In addition to the polarization-dependent Bragg grating for the main polarization mode selection of the GC, the high PER is also related to the birefringence characteristics introduced by the PMF itself and the femtosecond laser-induced Bragg gratings.

3.3. Linewidth characteristics

The linewidth characteristics of the laser were characterized using the delayed self-heterodyne technique [35,36], and the experimental setup is shown in Fig. 7. The light of the ECSL is divided into probe light and reference light after passing through an optical isolator (ISO), and a 90/10 beam coupler (C1) is used to allow more light to enter the delay fiber. One beam of light passes through an acoustic optical modulator (AOM) (AA OPTO, MT80), which produces a frequency shift of 80 MHz, while the other beam of light is delayed by a 20 km delay fiber and a Faraday rotating mirror (FRM) and then injected into the combiner (C2) through a circulator. A delay path of 40 km achieves a delay of 0.20 ms, while the frequency shift of the signal induced by the AOM reduces the impact of technical noise caused by electrons, vibrations, and other environmental factors near the zero frequency on the beat frequency. The FRM can reflect incident light in an orthogonal polarization direction of 90°, which makes the polarization states of the two combined beams perpendicular to each other, minimizing the influence of thermal and mechanical disturbances in the fiber on the polarization state [37]. The photoelectric conversion is carried out by a photodetector (PD) (Menlo Systems, FPD310) after mixing the two beams of light, and then, the data are processed by an electrical spectrum analyser (ESA) (GW INSTEK, GPS9300) to obtain beat frequency results.

The beat spectra at different currents from the delayed self-heterodyne beat measurement are shown in Fig. 8 (a), and the thin red lines are fitted using Lorentz fitting. The full width at half maximum (FHWM) of the fitted curve is selected as the test result for the linewidth. The red circles in Fig. 8 (b) show the Lorentz linewidth measured under different currents, with a minimum value of 2.58 kHz, and the black line is the fitting curve of the measurement results. The blue line is the calculated result of the linewidth as a function of the injection current. It is considered to correspond to a combination of the active region and the passive external cavity and is obtained through the equivalent F-P resonant cavity model constructed in the previous laser structure section. The resonant cavity is considered to be an isolated laser with a fixed mode spacing based on the modified Schawlow-Townes equation, with which the numerical relationships between linewidth and injection current is calculated. The linewidth decreases with increasing injection current, and the slight deviation between the measured value and the fitting curve may come from the influence of the environmental acoustic oscillations on the linewidth measurement accuracy and the error introduced during the test or curve fitting. An increase in the output power helps narrow the linewidth. In addition, expansion of the cavity length improves the Q factor and photon lifetime of the resonant cavity, and it can also achieve effective linewidth narrowing.

3.4. Long-term output power characteristics

In addition, the long-term output power of the ECSL was also characterizated. Long-term monitoring of the power stability of the laser could be carried out using a power meter (Thorlabs, PM400). The monitoring time was 1800 s, and the sampling interval was 1 s. The laser stays away from the mode hopping point at an injection current of 225 mA and maintains a stable output state. The measured average power of

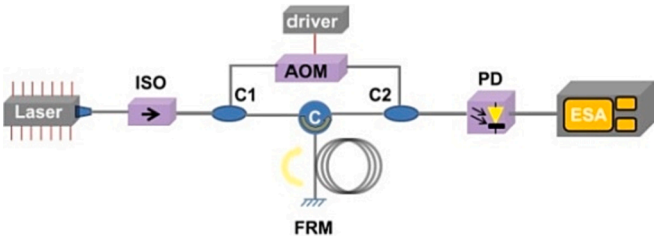

Fig. 7. Schematic of the laser linewidth measurement.

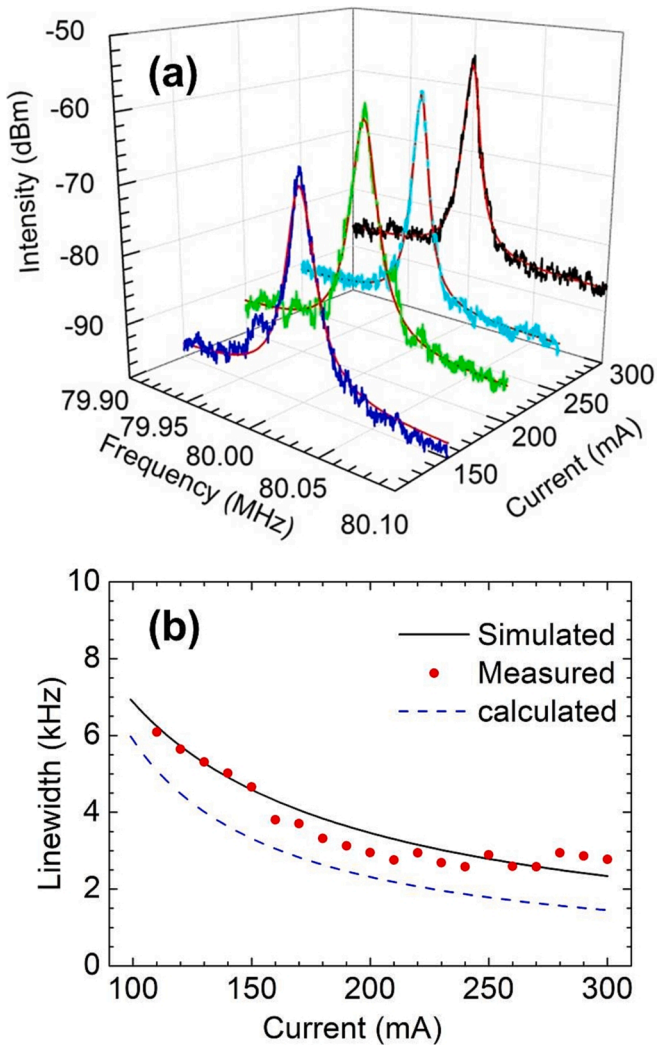

Fig. 8. (a) Measurement and fitting curves of the delayed self-heterodyne beat frequency. (b) Simulation and test results of the linewidth under different currents.

the laser is 30.45 mW, as shown in Fig. 9, while the standard deviation of the power fluctuation is 0.019. Therefore, the laser can be considered to maintain a stable long-term output power.

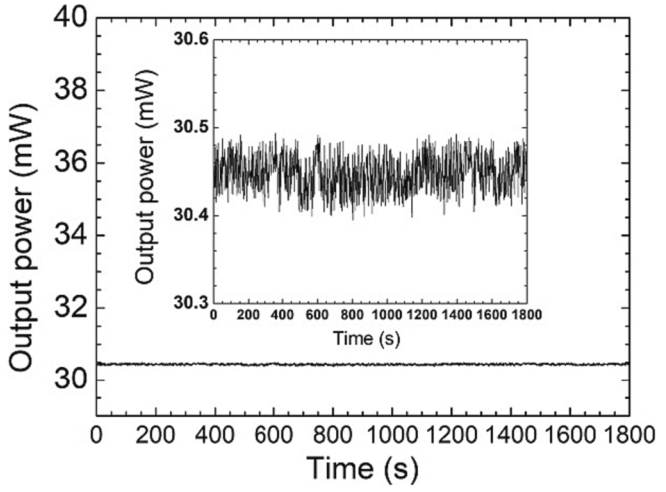

Fig. 9. Long-term output power of the ECSL.

4. Discussion

The statistics of some lasers and their corresponding characteristics for quantum precision measurement applications are shown in Table 1 [8–15]. DBR [9] and DFB [8] lasers typically have a PER of about 18 ± 2 dB; the external cavity structures can achieve a higher PER, but it is only 23 dB [13]; while our ECSL achieved a PER of over 30 dB, based on the orthogonal polarization eigenmode and effective selection of the external-cavity mode for the birefringent FBG, which is 5 times higher than the VHG-ECSL [13]. Besides, our ECSL also has significant advantages in linewidth characteristics. Although it does not reach the 80 Hz ultra-narrow linewidth of the WGM-ECSL [15]; our ECSL has excellent overall performance, especially with an output power of 60 mW, which is 30 times higher than that of the WGM-ECSL [15]. In terms of output power and SMSR, they are not as excellent as linewidth and PER. This will also become the focus of our next work.

5. Conclusions

In conclusion, we demonstrate an ECSL based on a birefringent Bragg grating and a ridge waveguide emission GC. The narrow-linewidth and linear polarization laser output achieved is due to the main polarization mode selection and external-cavity feedback provided by the birefringent grating induced by a femtosecond laser for the GC. This compact laser achieves an output power of > 60 mW and a PER of > 30 dB. The Lorentz linewidth measured by the delayed self-heterodyne beat frequency is 2.58 kHz. We present a narrow-linewidth and linear polarization ECSL for quantum precision measurement applications such as atomic clocks and atomic gyroscopes with a flexible and low-cost process, which provides a candidate scheme for batch preparation of compact light sources in other wavebands.

CRediT authorship contribution statement

Jiaqi Chen: Methodology, Investigation, Writing – original draft. **Chao Chen:** Conceptualization, Methodology, Validation, Writing – original draft, Writing – review & editing. **Qi Guo:** Formal analysis. **Jingjing Sun:** Formal analysis. **Jianwei Zhang:** Data curation. **Yinli Zhou:** . **Zhaohui Liu:** Visualization. **Yongsen Yu:** Formal analysis. **Li Qin:** Supervision. **Yongqiang Ning:** Project administration. **Lijun Wang:** Resources.

Declaration of Competing Interest

The authors declare that they have no known competing financial

Table 1
Statistics of some laser structures.

Setup	Linewidth	PER	Output power	SMSR	Wavelength
DFB [8]	500 kHz	—	48 mW	50 dB	894 nm
DBR [9]	500 kHz	16 dB	20 mW	30 dB	852 nm
Littrow-ECSL [10]	87 kHz	—	50 mW	—	780 nm
IF-ECSL [11]	28.3 kHz	—	30 mW	—	852 nm
Cateye ECSL [12]	100 kHz	20 dB	200 mW	—	780 nm
VHG-ECSL [13]	100 kHz	23 dB	50 mW	50 dB	780 nm
VHG-ECSL[14]	19 kHz	—	30 mW	—	780 nm
WGM ECSL [15]	80 Hz	20 dB	2 mW	50 dB	780 nm
PM-FBG-ECSL (This work)	2.58 kHz	30 dB	61 mW	55 dB	852 nm

*The full names of abbreviations of optical components in Table 1. IF: interference filter, WGM: whispering gallery mode, VHG: volume holographic grating.

interests or personal relationships that could have appeared to influence the work reported in this paper.

Data availability

Data will be made available on request.

Acknowledgements

This work is supported by the National Natural Science Foundation of China (62374164, 62090060, 62090064, 62174046, 62305130), Science and Technology Development Project of Jilin Province (20220201063GX), Changchun Science and Technology Development Plan Project (22SH01), and Finance Science and Technology Project of Hainan Province (ZDYF2020217).

Institutional Review Board Statement

Not applicable.

***Informed Consent** Statement*

Not applicable.

References

[1] C.W. Chou, D.B. Hume, T. Rosenband, D.J. Wineland, Optical clocks and relativity, Science 329 (5999) (2010) 1630–1633.
[2] E. Luvsandamdin, S. Spießberger, M. Schiemangk, A. Sahm, G. Mura, A. Wicht, A. Peters, G. Erbert, G. Tränkle, Development of narrow linewidth, micro-integrated extended cavity diode lasers for quantum optics experiments in space, Appl. Phys. B 111 (2) (2013) 255–260.
[3] N. Yu, J.M. Kohel, J.R. Kellogg, L. Maleki, Development of an atom-interferometer gravity gradiometer for gravity measurement from space, Appl. Phys. B 84 (2006) 647–652.
[4] A.D. Ludlow, T. Zelevinsky, G.K. Campbell, S. Blatt, M.M. Boyd, M.H.G. de Miranda, M.J. Martin, J.W. Thomsen, S.M. Foreman, T.M. Jun Ye, J.E. Fortier, S. A. Stalnaker, Y.L. Diddams, Z.W. Coq, N. Barber, N.D. Poli, K.M. Lemke, C.W. Beck, Oates,, Sr lattice clock at 1×10^{-16} fractional uncertainty by remote optical evaluation with a Ca clock, Science 319 (2008) 1805–1808.
[5] H. Shi, P. Chang, Z. Wang, Z. Liu, T. Shi, J. Chen, Frequency stabilization of a Cesium Faraday laser with a double-layer vapor cell as frequency reference, IEEE Photonics J. 14 (6) (2022) 1561006.
[6] M.T. Hummon, S. Kang, D.G. Bopp, Q. Li, D.A. Westly, S. Kim, C. Fredrick, S. A. Diddams, K. Srinivasan, V. Aksyuk, J.E. Kitching, Photonic chip for laser stabilization to an atomic vapor with 10^{-11} instability, Optica 5 (4) (2018) 443–449.
[7] C.H. Henry, Theory of the linewidth of semiconductor lasers, IEEE J. Quant. Electron 18 (1982) 259–264.
[8] M. Krakowskia, M. Meghnagia, P. Afuso-Roxoa, B. Vintera, F. Duporta, F. Dijka, A. Larruea, C. Theveneaua, E. Vineta, Y. Roberta, J.P. Legoeca, M. Garciaa, O. Parillauda, B. Gerard, Modulated DFB-ridge laser diodes at 894 nm for compact Cesium CPT atomic clocks, proc, SPIE (2023) 12440.
[9] Photodigm, "852 nm Laser Diode | PH852DBR Series", datasheet (2018), https://www.photodigm.com/products/852-nm-laser-diode.
[10] S.D. Saliba, R.E. Scholten, Linewidths below 100 kHz with external cavity diode lasers, Appl. Opt. 48 (36) (2009) 6961–6966.
[11] Z. Jiang, Q. Zhou, Z. Tao, X. Zhang, S. Zhang, C. Zhu, P. Lin, J. Chen, Diode laser using narrow bandwidth interference filter at 852 nm and its application in Faraday anomalous dispersion optical filter, Chin. Phys. B 25 (8) (2016), 083201.
[12] MOGLabs, "External cavity diode laser", datasheet (2014) , https://www.moglabs.com/user/pages/03.products/02.ldl/MOGLabs_LDL_manual_rev207.pdf.
[13] A. Jiménez, T. Milde, N. Staacke, C. Aßmann, G. Carpintero, J. Sacher, Narrow-line external cavity diode laser micro-packaging in the NIR and MIR spectral range, Appl. Phys. B 123 (2017) 207.
[14] S. Yim, T. Kim, J. Choi, A simple extended-cavity diode laser using a precision mirror mount, Rev. Sci. Instrum. 91 (2020), 046102.
[15] OEwaves, "HI-Q™ near IR laser", datasheet (2015), https://www. oewaves.com/oe4078.
[16] C. Diboune, N. Zahzam, Y. Bidel, M. Cadoret, A. Bresson, Multi-line fiber laser system for cesium and rubidium atom interferometry, Opt. Express 25 (15) (2017) 16898–16906.
[17] H. Shang, T. Zhang, J.X. Miao, T.T. Shi, D. Pan, X.W. Zhao, Q. Wei, L. Yang, J. B. Chen, Laser with 10^{-13} short-term instability for compact optically pumped cesium beam atomic clock, Opt. Express 28 (5) (2020) 6868–6880.
[18] M. Wahbeh, R. Kashyap, Purity of the single frequency mode of a hybrid semiconductor-fiber laser, Opt. Express 23 (12) (2015) 16084–16095.
[19] X. Luo, X. Chen, L. Qin, X. Zhang, Y. Chen, B. Wang, L. Liang, P. Jia, Y. Ning, L. Wang, High-birefringence waveguide Bragg gratings fabricated in a silica-on-silicon platform with displacement Talbot lithography, Opt. Mater. Express 10 (10) (2022) 2406–2414.
[20] J. Burgmeier, C. Waltermann, G. Flachenecker, W. Schade, Point-by-point inscription of phase-shifted fiber Bragg gratings with electro-optic amplitude modulated femtosecond laser pulses, Opt. Lett. 39 (3) (2014) 540–543.
[21] N. Jovanovic, J. Thomas, R.J. Williams, M.J. Steel, G.D. Marshall, A. Fuerbach, S. Nolte, A. Tünnermann, M.J. Withford, Polarization- dependent effects in point-by-point fiber Bragg gratings enable simple, linearly polarized fiber lasers, Opt. Express 17 (8) (2009) 6082–6095.
[22] M.I. Skvortsov, A.A. Wolf, A.V. Dostovalov, A.A. Vlasov, V.A. Akulov, S.A. Babin, Distributed feedback fiber laser based on a fiber Bragg grating inscribed using the femtosecond point-by-point technique, Laser Phys. Lett. 15 (2018), 035103.
[23] L. Hao, X. Wang, K. Jia, G. Zhao, Z. Xie, S. Zhu, Narrow-linewidth single-polarization fiber laser using non-polarization optics, Opt. Lett. 46 (15) (2021) 3769–3772.
[24] L.A. Coldren, S.W. Corzine, M.L. Masanovic, Diode lasers and photonic integrated circuits, 2nd edn., Wiley, Canada, 2012.
[25] H.K. Hisham, G.A. Mahdiraji, A.F. Abas, M.A. Mahdi, F.R.M. Adikan, Linewidth optimization in fiber grating Fabry-Perot laser, Opt. Eng. 53 (2) (2014), 026107.
[26] L.Y. Karachinsky, I.I. Novikov, Y.M. Shemyakov, S.M. Kuznetsov, N.Y. Gordeev, M. V. Maximov, P.S. Kop'ev, High power GaAs/AlGaAs lasers (λ=850 nm) with ultranarrow vertical beam divergence, Appl. Phys. Lett. 89 (23) (2006) 23114.
[27] F.J. Vermersch, V. Ligeret, S. Bansropun, M. Lecomte, O. Parillaud, M. Calligaro, M. Krakowski, G. Giuliani, High-power narrow linewidth distributed feedback lasers with an Aluminium-free active region emitting at 852 nm, IEEE Photon. Technol. Lett. 20 (13) (2008) 1145.
[28] R. Lv, T. Chen, X. Pham, J. Si, J. Huang, Y. Hou, B. Gao, X. Hou, High-temperature linearly polarized single-frequency fiber lasers based on a non-polarization-maintaining FBG preparation through a femtosecond laser, Opt. Lett. 47 (16) (2022) 4111–4114.
[29] X. Luo, X. Chen, Y. Ning, J. Zhang, J. Chen, X. Zhang, L. Li, H. Wu, Y. Zhou, L. Qin, L. Wang, Single polarization, narrow linewidth hybrid laser based on selective polarization mode feedback, Opt. Laser Technol. 154 (2022), 108340.
[30] Y. Wang, H. Tai, R. Duan, M. Zheng, W. Lu, Y. Shi, J.W. Zhang, X. Zhang, Y. Q. Ning, J. Wu, Super-gain nanostructure with self-assembled well-wire complex energy-band engineering for high performance of tunable laser diodes, Nanophotonics 12 (9) (2023) 1763–1776.
[31] R.J. Williams, R.G. Kramer, S. Nolte, M.J. Withford, M.J. Steel, Detuning in apodized point-by-point fiber Bragg gratings: insights into the grating morphology, Opt. Express 21 (22) (2013) 26854–26867.
[32] M. Malinauskas, A. Žukauskas, S. Hasegawa, Y. Hayasaki, V. Mizeikis, R. Buividas, S. Juodkazis, Ultrafast laser processing of materials: from science to industry, Light Sci. Appl. 5 (2016) e16133.
[33] W. He, J. Hu, S. Li, H. Liu, S. Ma, L. Zhu, Femtosecond laser-inscribed polarization-maintaining fiber Bragg grating using line-by-line technique for generating wavelength-switchable erbium-doped fiber lasers, Opt. Fiber Technol. 78 (2023), 103327.
[34] Y. Lai, K. Zhou, K. Sugden, I. Bennion, Point-by-point inscription of first-order fiber Bragg grating for C-band applications, Opt. Express 15 (26) (2007) 18318–18325.
[35] Z. Wang, C. Ke, Y. Zhong, C. Xing, H. Wang, K. Yang, D. Liu, Ultra-narrow-linewidth measurement utilizing dual-parameter acquisition through a partially coherent light interference, Opt. Express 28 (6) (2020) 8484–8493.
[36] S. Bennetts, G.D. McDonald, K.S. Hardman, J.E. Debs, C.C.N. Kuhn, J.D. Close, N. P. Robins, External cavity diode lasers with 5kHz linewidthand 200 nm tuning range at 1.55 um and methodsfor linewidth measurement, Opt. Express 22 (9) (2014) 10642–10654.
[37] A. Canagasabey, A. Michie, J. Canning, J. Holdsworth, S. Fleming, H.C. Wang, M. L. Åslund, A comparison of Michelson and Mach-Zehnder interferometers for laser linewidth measurements, IQEC/CLEO Pacific Rim (2011) 1392–1394.